

Asymmetrical meridional expansion of bright clouds from Saturn's 2010 great white storm

Liming Li^{a,*}, Aaron Studwell^b, Timothy E. Dowling^c, Mary E. Bradley^d, Ellen C. Crecy^b, Ronald J. Albright^b, Xun Jiang^b

^a Department of Physics, University of Houston, Houston, TX, United States of America

^b Department of Earth and Atmospheric Sciences, University of Houston, Houston, TX, United States of America

^c Department of Physics and Astronomy, University of Louisville, Louisville, KY, United States of America

^d Department of Mathematics, University of Louisville, Louisville, KY, United States of America

ABSTRACT

Saturn's recurring great white storms play an important role in modifying its atmosphere. In 2010, such a storm with clouds encircling the planet occurred in the northern hemisphere. An interesting phenomenon of this storm is that the associated bright clouds expanded asymmetrically with respect to latitude, such that the southern boundary of the bright clouds moved ~ 2.7 times as far as the northern boundary during an 8-month period. Based on the wind and temperature fields retrieved from the Cassini visible and infrared observations, we explore the mechanism behind this asymmetrical expansion. Our analysis shows that the northern edge, which quickly stopped moving, coincides with the largest meridional gradient of the quasi-geostrophic potential vorticity (PV) in the region of interest, which is coincident with the strongest jet in the region, suggesting this forms an effective barrier to meridional transport, much like a polar vortex. In contrast, the storm's southern edge, which kept moving, passed through weaker PV gradients and jets. For the threshold value of the meridional gradient of PV needed to form an effective barrier to meridional transport in Saturn's mid-latitude upper-troposphere, we estimate lower and upper bounds of $\sim 2.1 \times 10^{-11} \text{ m}^{-1} \text{ s}^{-1}$ and $\sim 3.6 \times 10^{-11} \text{ m}^{-1} \text{ s}^{-1}$.

1. Introduction

Saturn's great white storms generate bright clouds covering a large fraction of a longitudinal circle or even encircling the planet. They occur in either hemisphere and appear to be seasonal, erupting typically once per Saturnian year (Sanchez-Lavega et al., 2012; Li and Ingersoll, 2015). In 2010, such a storm formed in the northern hemisphere and was well characterized by the Cassini orbiter and ground-based observations (Sanchez-Lavega et al., 2011; Fischer et al., 2011; Fletcher et al., 2011). Interestingly, this storm's bright clouds expanded meridionally much more to the south than to the north. This asymmetry was noticeably pronounced by the time the bright clouds encircled the whole planet, as discussed in previous studies (Sanchez-Lavega et al., 2011, 2012; Sayanagi et al., 2013; Garcia-Melendo et al., 2013). In this article we explore a possible mechanism behind the asymmetric expansion.

Fig. 1 shows the time series of maps of the 2010 great white storm, which are recorded by the second continuum filter (CB2 $\sim 752 \text{ nm}$) of the Imaging Science Sub-system (ISS) (Porco et al., 2004) onboard the Cassini spacecraft. Based on Fig. 1, the bright clouds generated by the storm expand not only in the longitudinal direction but also in the latitudinal direction (in this article, west longitude and planetographic

latitude are used). To determine the boundary of bright clouds in the latitudinal direction, we select the longitudinal sections of the bright clouds and calculate the standard deviation of brightness in the longitudinal direction for each latitude. Saturn's atmosphere has a banded structure, in which the cloud brightness is relatively uniform in the longitudinal direction. The standard deviation in the longitudinal direction is larger in the region of bright clouds than in the relatively uniform regions which were not disturbed by the storm and its related clouds, so we use the minimum of the standard deviation to determine the boundary of the bright clouds in the meridional direction. It should be mentioned that the standard deviation of the banded areas that are not affected by the storm also oscillates, mainly because of the alternating zones and belts, so there are multiple minima and maxima in the meridional direction (see panels F, G, H, I, and J of Fig. 1). Therefore, we first determine the rough position of the latitudinal boundary of bright clouds by visual inspection of the visible maps shown in Fig. 1 and then use the minimum of the standard deviation near the rough position to precisely determine the latitudinal boundary of bright clouds.

Panel A of Fig. 1 suggests that strong divergence at the storm head, which is related to upwelling, spread the bright clouds until they spanned the latitudes $\sim 31^\circ \text{N}$ to $\sim 45^\circ \text{N}$ (panel F). Then, the zonal winds

* Corresponding author.

E-mail address: lli7@central.uh.edu (L. Li).

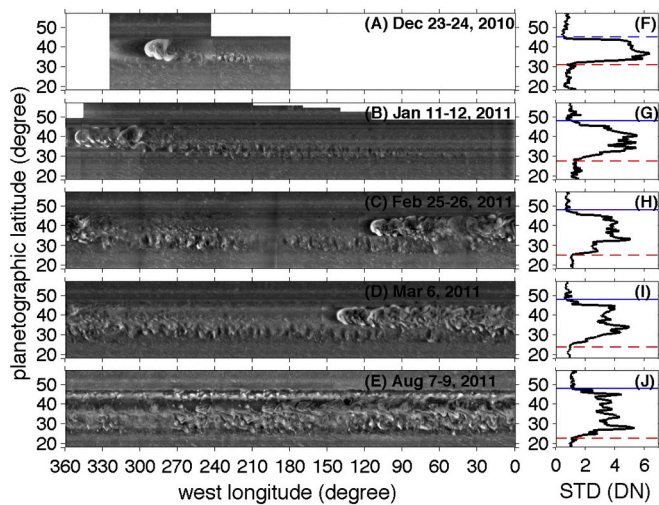


Fig. 1. Time series of projected maps for the 2010 great white storm. The raw ISS image were taken by the Cassini ISS wide-angle camera in the second continuum band (CB2, 752 nm) with a spatial resolution ranging from ~ 50 km/pixel to ~ 150 km/pixel. The blank areas in panels A and B are observational gaps. Panels A-E are the time series of the images of the 2010 storm, and the brightness of images was recorded by the Cassini/ISS with a unit of digital number (DN). Panels F-J are the standard deviations (STD) of DN in the longitude direction for the images shown in panels A-E, respectively. The local minimum of STD is used to determine the latitudinal boundaries of the bright clouds from the 2010 storm (see discussion in the text). Horizontal blue and red lines in panels F-J represent the northern and southern boundaries of the bright clouds from the 2010 storm, respectively. The instantaneous northern boundary in panel F ($\sim 45^\circ\text{N}$) is represented by the horizontal blue dashed line. This boundary ($\sim 45^\circ\text{N}$) moved to $\sim 48^\circ\text{N}$ in panel G and then stopped (see panels H-J); the solid horizontal blue lines in panels G-J signify that the northern boundary no longer moved with time. On the other hand, the southern boundary (i.e., the horizontal red dashed line) kept moving from 31°N (panel F) to 27°N (panel G) to 25°N (panel H) to 24°N (panel I) and finally to 23°N (panel J). (For interpretation of the references to colour in this figure legend, the reader is referred to the web version of this article.)

advected the bright clouds in the longitudinal direction and developed them into a planet encircling bright-cloud zone. The northern boundary of the bright-cloud zone moved $\sim 3^\circ$, from $\sim 45^\circ\text{N}$ in December 2010 (panel F) to $\sim 48^\circ\text{N}$ in January 2011 (panel G), and then kept stable with time (see panels H, I, and J). On the other hand, the southern boundary steadily moved $\sim 8^\circ$, from $\sim 31^\circ\text{N}$ in December 2010 to $\sim 23^\circ\text{N}$ in August 2011 (see panels from F to J), such that during the 8-month period from December 2010 to August 2011, the bright clouds moved ~ 2.7 times more southward than northward. This asymmetrical meridional expansion may be due to north-south asymmetry in eddy mixing processes (e.g., Polvani et al., 1995; McIntyre, 2014), which are affected by meridional potential vorticity gradients. A possible alternative to a large PV gradient is a strong zonal jet (Beron-Vera et al., 2012). We consider both possibilities, keeping in mind that for gas giants they can be two sides of the same coin (Dowling, 2019).

2. Methodology

The meridional gradient of the zonal-mean quasi-geostrophic potential vorticity is referred to as the effective beta in this article, β_e (and is also often written \bar{Q}_y). This is a central parameter in atmospheric dynamics because an environmental gradient in potential vorticity gives rise to Rossby waves, which are potential-vorticity conserving waves that control much of the dynamics of large-scale flows (Pedlosky, 1987; Andrews et al., 1987; Salby, 1996; Holton and Hakim, 2013). The effective beta has previously been analyzed in studies of Saturn's atmosphere (e.g., Read et al., 2009a, 2009b). We recalculate it here using

observations taken during the 2010 storm, because it has been found empirically and theoretically that a sufficiently large magnitude of β_e acts like a transport barrier to inhibit meridional cloud mixing (e.g., Polvani et al., 1995; McIntyre, 2014).

The effective beta consists of three distinct terms (Andrews et al., 1987; Salby, 1996),

$$\beta_e = \beta + \beta_y + \beta_z \quad (1)$$

where the first, β , is the meridional gradient of the planetary vorticity, $f = 2\Omega\sin\phi$, where Ω is the rotation rate of Saturn and ϕ is planetographic latitude, and hence can be expressed as

$$\beta = \frac{df}{dy} = \frac{1}{R} \frac{df}{d\phi} = \frac{1}{R} 2\Omega \cos\phi \quad (2)$$

where $R(\phi) = r_e^2 r_p^2 \left[(r_e \cos\phi)^2 + (r_p \sin\phi)^2 \right]^{-3/2}$ is the local meridional radius of curvature, taking into account Saturn's oblate shape, and r_e and r_p are the planet's equatorial and polar radii, respectively. We use 60,268 km and 54,364 km for the values of r_e and r_p respectively, which are provided by NASA (<https://nssdc.gsfc.nasa.gov/planetary/factsheet/saturnfact.html>). The second term in (1), β_y , is the meridional gradient of the zonally averaged relative vorticity, $\bar{\zeta}$, which is sometimes expressed for convenience in the Cartesian form “ $-\bar{u}_{yy}$ ”, where \bar{u} is the zonally averaged zonal wind, but is calculated here with oblate-spherical map factors as

$$\beta_y = \frac{1}{R} \frac{d\bar{\zeta}}{d\phi}; \bar{\zeta} = -\frac{1}{rR} \frac{d(r\bar{u})}{d\phi} \quad (3)$$

where $r(\phi) = r_e^2 \cos\phi \left[(r_e \cos\phi)^2 + (r_p \sin\phi)^2 \right]^{-1/2}$ is the local zonal radius of curvature. A Savitsky-Golay filter with second-order smoothing polynomials and 11-point weighted average is applied to the zonal-wind profile before computing the relative vorticity (see Dowling, 1995). The third term in (1), β_z , is the meridional gradient of the quasi-geostrophic stretching vorticity, which in pressure coordinates may be written (Holton and Hakim, 2013, p. 207) as

$$-\frac{\partial}{\partial p} \left(\frac{f}{\sigma_0} \alpha \right); \alpha = \frac{R_{\text{gas}} T}{p} \quad (4)$$

where $\sigma_0(p) = - (R_{\text{gas}} T_0/p) \ln \theta_0/p$ is a reference static-stability profile versus pressure, based on reference profiles of temperature and potential temperature, $T_0(p)$ and $\theta_0(p)$. For consistency in the quasi-geostrophic scheme, the factor (f/σ_0) in (4) does not participate in the meridional gradient, such that

$$\beta_z = -\frac{f}{R} \frac{\partial}{\partial p} \left(\frac{1}{\sigma_0} \frac{\partial \alpha}{\partial \phi} \right) \quad (5)$$

The temperature data needed in (4) and (5) for the specific volume, α , for the 2010 storm were measured by the Composite Infrared Spectrometer (CIRS) onboard Cassini as described below.

3. Results

The Cassini spacecraft not only recorded the expansion of the bright clouds from the 2010 storm (Fig. 1) but also provided the observations and measurements to estimate the three terms that make up β_e . For the first term, β , we need Saturn's rotation rate, Ω , which has historically been difficult to determine because the angle between the planet's rotational and magnetic-dipole axes does not exceed 0.007° (Cao et al., 2019). We adopt the System IIIw rotation period of 10 h 34 min 13 s (Read et al., 2009b), with the corresponding rotation rate $\Omega = 1.651 \times 10^{-4} \text{ s}^{-1}$.

For the second term, β_y , we need the zonal winds at the pressure level of these bright clouds from the 2010 storm to estimate the meridional

gradient of the relatively vorticity (3). The bright clouds from the 2010 storm are located around 400 hPa (Garcia-Melendo et al., 2013; 1 hPa = 1 mbar). These bright clouds were recorded using the Cassini ISS CB2 filter, and the same ISS images were used to measure the zonal winds (e. g., Sayanagi et al., 2013), such that the winds correspond to the same time and pressure levels as the bright clouds. Panel A of Fig. 2 shows the profile of zonal winds from a previous study (Sayanagi et al., 2013), which includes the latitude band of the 2010 storm. The original zonal winds in the study by Sayanagi et al. (2013) have a spatial resolution 0.1 degree. We first average the 0.1-degree winds to 1-degree winds and then apply a Savitsky-Golay filter to further smooth the wind profile (see panel A of Fig. 2). Based on the filtered winds, we calculate β_y , which is shown in panel B of Fig. 3. The uncertainty in β_y mainly comes from the uncertainty in the zonal winds. The uncertainty of zonal winds was estimated as $\sim 1.7\text{--}4.3\text{ ms}^{-1}$ (Sayanagi et al., 2013), which varies with latitude (see panel A of Fig. 2). Based on the error propagation theory (Bevington and Robinson, 2003), we substitute the uncertainty of zonal winds into the equation of β_y to generate the uncertainty in β_y (see panel B of Fig. 3).

To calculate the third term, β_z , which involves vertical derivatives with respect to pressure of functions of temperature (5), we need atmospheric temperatures in a pressure interval that appropriately brackets the wind pressure level. The Cassini CIRS instrument provided infrared spectra that were used to retrieve these temperatures (Flasar et al., 2004). Here, we use Saturn's atmospheric temperature in 2011 (Achterberg et al., 2014), which is shown in panel B of Fig. 2. The 2010 storm erupted in the end of 2010 and continued to develop in 2011, so

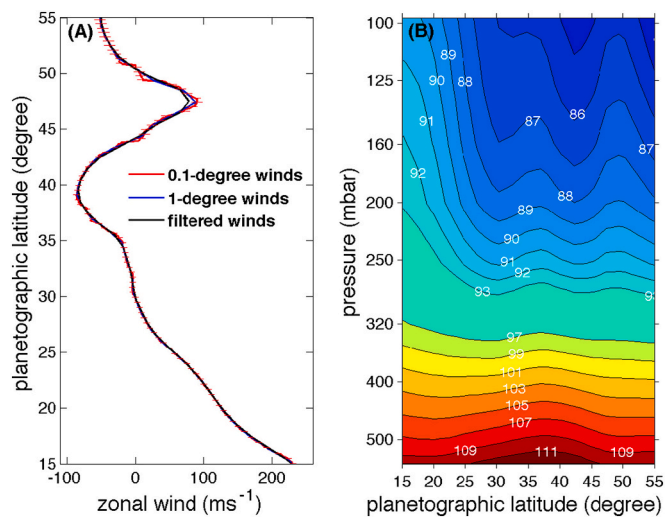


Fig. 2. The Cassini measurements of atmospheric wind and temperature fields of Saturn. (A) Zonal winds in 2011. The zonal winds come from a previous study by Sayanagi et al. (2013), which are based on the Cassini/ISS observations in January and August 2011. The original data (Sayanagi et al., 2013) are referenced to Saturn's rotation rate from the Voyager observations ($\Omega = 1.638 \times 10^{-4}\text{ s}^{-1}$). To be consistent with our analysis based on the System IIIw rotation rate ($\Omega = 1.651 \times 10^{-4}\text{ s}^{-1}$; Read et al., 2009b), we convert the data to the System IIIw rotation rate. The original data of zonal winds have a spatial resolution $\sim 0.1^\circ$ in latitude (i.e., 0.1-degree winds represented by the red line in panel A), and the uncertainty of measured winds was estimated to be in the range of $1.7\text{--}4.2\text{ ms}^{-1}$ (i.e., horizontal error-bars around the red line in panel A). We average the data with a latitude bin of 1° (i.e., 1-degree winds represented by the blue line in panel A), and then filter variations at small spatial scales (i.e., filtered winds represented by the black line in panel A). (B) Temperature in 2011. The original atmospheric temperature data come from a previous study by Achterberg et al. (2014), which were retrieved from Cassini/CIRS 2011 observations, which have a spatial resolution $\sim 1^\circ$ in latitude and ~ 0.1 scale height in the vertical direction. The numbers in the contour lines are in Kelvin. (For interpretation of the references to colour in this figure legend, the reader is referred to the web version of this article.)

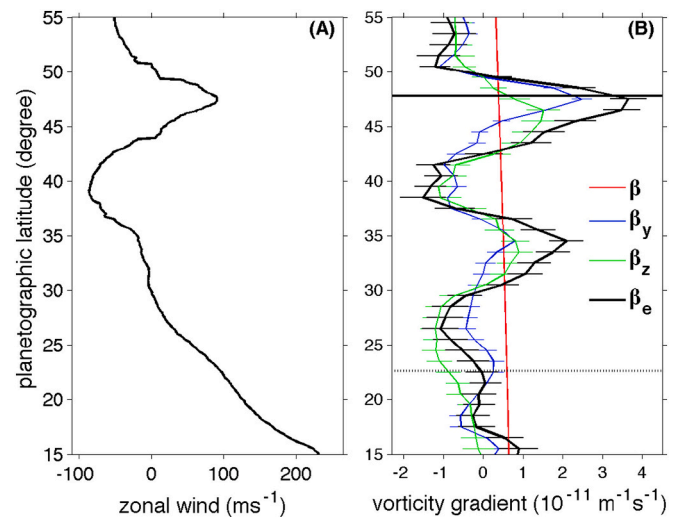


Fig. 3. Comparison between the zonal winds and the meridional gradient of the quasi-geostrophic potential vorticity. (A) Zonal winds. This profile comes from panel A of Fig. 2 (0.1-degree winds). (B) Effective beta (β_e) and its constituent terms (β , β_y , and β_z). The horizontal short line around the profiles of β_y , β_z , and β_e represent the corresponding uncertainties (see discussion in the text). The long horizontal solid line represents the final northern boundary of the bright clouds from the 2010 great white storm, and the horizontal dashed line stands for the southern boundary of the bright clouds shown by panel J of Fig. 1. Considering that the southern boundary kept moving during the observational period, such a boundary is possibly not the final boundary.

the period of these CIRS-retrieved temperatures is consistent with the mature 2010 storm. Panel B of Fig. 2 displays the atmospheric temperatures in the upper troposphere ($\sim 100\text{--}500$ hPa), which bracket the ~ 400 hPa pressure level of the 2010 bright clouds. The pressure derivatives for σ_0 and β_z were calculated via finite differencing using the pressure levels 345 hPa, 403 hPa, and 453 hPa. See the Supporting Information for details on the evaluation of the thermodynamical parameters (e.g. R_{gas} and c_p) needed to calculate α , σ_0 , and θ_0 for this region of Saturn's atmosphere. The results for β_z and the full potential vorticity gradient, β_e , are shown in Fig. 3.

Next we estimate the uncertainty in the gradient of the stretching vorticity, β_z , which mainly depends on temperature. The uncertainty in the CIRS-retrieved temperature is $\sim 1\text{ K}$ (Fletcher et al., 2010). With the error propagation (Bevington and Robinson, 2003), such an uncertainty is substituted into the equation of β_z to estimate the uncertainty in β_z . Panel B of Fig. 3 shows that the uncertainty is larger in β_z than in β_y for most latitudes. Assuming uncorrelated errors, the square root of the sum of the squares of the uncertainties of β_y and β_z is used to represent the uncertainty in β_e (Bevington and Robinson, 2003), which is also shown in panel B of Fig. 3.

A comparison between the structure of the environmental potential vorticity gradient, β_e , and the observed asymmetrical meridional expansion of the 2010 bright clouds can now be made. Panel B of Fig. 3 shows that in the region of interest, β_e has its strongest peak around 48°N ($\sim 3.6 \times 10^{-11}\text{ m}^{-1}\text{ s}^{-1}$), which corresponds to a strong eastward zonal jet at that latitude (panel A of Fig. 3). The core of the eastward zonal jet corresponds to the strongest β_y , which is the main contributor to the peak of β_e at 48°N . Significantly, the latitude with the peak β_e aligns with the sharply defined northern boundary of the bright clouds from the 2010 storm. We surmise that this peak value of β_e ($\sim 3.6 \times 10^{-11}\text{ m}^{-1}\text{ s}^{-1}$) is sufficient to inhibit meridional transport of the 2010 great white storm system. Furthermore, the lack of a similar stop to the southward expansion of the bright clouds provides complementary information on a possible threshold value for β_e needed to form an effective barrier. Specifically, the local extremum in β_e around 35°N ($\sim 2.1 \times 10^{-11}\text{ m}^{-1}\text{ s}^{-1}$) did not similarly inhibit the southward expansion of the bright

clouds. Such a local extremum comes from the local maxima of both β_y and β_z (see panel B of Fig. 3). The local maximum of β_y is related to a local inflexion of zonal winds around 35°N (panel A of Fig. 3), and is a robust feature seen in other studies (e.g., Sánchez-Lavega et al., 2000; García-Melendo et al., 2011; Sayanagi et al., 2013). Considering that the local extremum in β_e around 35°N ($\sim 2.1 \times 10^{-11} \text{ m}^{-1} \text{ s}^{-1}$) is roughly half the value of the extremum of β_e around 48°N ($\sim 3.6 \times 10^{-11} \text{ m}^{-1} \text{ s}^{-1}$), we suggest that the threshold for forming a meridional transport barrier lies between these values of β_e . This information could prove useful to the theoretical development of barriers to meridional transport (e.g., Polvani et al., 1995; McIntyre, 2014).

It is desirable to non-dimensionalize the PV barrier threshold estimate found here, so that the results can be generalized and applied to other situations and to other planets. Dritschel and McIntyre (2008) study how PV barriers inhibit meridional transport and find that “substantial penetration requires $\Delta q_{\text{vortex}} \geq \Delta q_{\text{barrier}}$, with an accuracy or fuzziness of order 10%,” where Δq_{vortex} is the PV anomaly (relative to the background) of a vortex and $\Delta q_{\text{barrier}}$ is the PV jump across the barrier. The associated non-dimensional barrier threshold is then $\Delta q_{\text{barrier}}^* \geq 1$, where $\Delta q_{\text{barrier}}^* = \Delta q_{\text{barrier}} / \max(\Delta q_{\text{vortex}})$. Now we consider two limits to the storm-related turbulence. At the larger end, we take the whole storm head as a vortex. Based on the vorticity measurements of the storm head provided by García-Melendo et al. (2013), we can estimate the vorticity gradient of the storm head as $(2.0 \times 10^{-4} \text{ m}^{-1} \text{ s}^{-1}) / (8 \times 10^6 \text{ m}) \approx 2.5 \times 10^{-11} \text{ m}^{-1} \text{ s}^{-1}$, where $2.0 \times 10^{-4} \text{ m}^{-1} \text{ s}^{-1}$ is the vorticity range for the storm head (see panel c in Fig. 3 of García-Melendo et al., 2013) and $8 \times 10^6 \text{ m}$ is the size of the storm head in the meridional direction (the storm head occupies 8 degrees in the meridional direction). Such a vorticity gradient ($2.5 \times 10^{-11} \text{ m}^{-1} \text{ s}^{-1}$) is smaller than the peak value of β_e around 48°N ($\sim 3.6 \times 10^{-11} \text{ m}^{-1} \text{ s}^{-1}$). It means that $\Delta q_{\text{barrier}}^* \geq 1$, which also suggests that the storm head cannot penetrate the barrier around 48°N. However, we think the more relevant limit is the smaller end. The vorticity fields of the separate cloud patches with much smaller sizes (~ 1 degree in latitude and longitude) probably play a more important role in the meridional movements of these bright clouds from the 2010 storm, but it is difficult to measure the high-spatial-resolution internal winds and hence vorticity fields of these small cloud patches. From $\Delta q_{\text{barrier}}^* \geq 1$ and the value of $\Delta q_{\text{barrier}}$, we have $\max(\Delta q_{\text{vortex}}) \leq 3.25 \times 10^{-11} \text{ m}^{-1} \text{ s}^{-1}$, which sets an upper criterion of vorticity gradient for the stability of the bright cloud patches from the 2010 storm. Taking into account the nuances related to the size of penetrating vortices detailed by Dritschel and McIntyre (2008), on the whole their work indicates that when an environmental PV barrier is resolved by observations, as is the case here, then it provides a useful PV-anomaly constraint on unresolved turbulence.

4. Conclusions and discussions

In this study, we calculated the effective beta (i.e., the meridional gradient of zonal-mean quasi-geostrophic potential vorticity) based on

wind and temperature fields associated with the environment of the 2010 great white storm on Saturn, which were retrieved from contemporaneous Cassini observations. The analysis of effective beta suggests that the threshold for forming a barrier to meridional transport in the region of Saturn's 2010 storm (i.e., $\sim 23\text{--}48^\circ\text{N}$) lies between $\sim 2.1 \times 10^{-11} \text{ m}^{-1} \text{ s}^{-1}$ and $\sim 3.6 \times 10^{-11} \text{ m}^{-1} \text{ s}^{-1}$. A non-dimensional parameter is further suggested to facilitate the analysis of the meridional movement of vortices and clouds on other planets.

The physical mechanisms that associate a large meridional gradient of quasi-geostrophic potential vorticity with a meridional transport barrier have been primarily developed for Earth's stratosphere (e.g., Polvani et al., 1995). For the underlying troposphere, it is not easy to identify the potential-vorticity gradient mechanism because Earth's troposphere has more complicated dynamics than the stratosphere (e.g., planetary boundary layer). In this light, it may be significant that the troposphere of Saturn has a relatively simple dynamical environment with no terrestrial-style planetary boundary layer. In other words, the potential-vorticity gradient mechanism may be less obscured in gas-giant tropospheres compared to solid-planet tropospheres.

As mentioned in the introduction, the necessity of large potential vorticity gradients in the formation of meridional barriers has recently been challenged in the terrestrial literature; the alternative hypothesis is that a strong eastward or westward zonal jet itself is the important attribute, regardless of the associated potential vorticity gradient (Berón-Vera et al., 2012). On Jupiter and Saturn, the large positive and negative potential vorticity gradients tend to correlate with large eastward and westward zonal-jet speeds, respectively (Dowling, 2020), which is consistent with our results. In this case, an effective barrier to meridional transport, which plays an important role in the evolution of major convective storms, can be characterized either way on gas giants.

Declaration of Competing Interest

None.

Acknowledgments

We gratefully acknowledge the Cassini ISS team for publicizing data sets, Dr. Richard Achterberg and Dr. Kunio Sayanagi for providing the Cassini/CIRS temperature and the Cassini/ISS winds from their publications, and Dr. Achterberg and Dr. Lawrence Sromovsky for constructive discussions on the clouds and basic parameters of Saturn's atmosphere. We also thank two anonymous reviewers for their constructive suggestions to improve the manuscript. LL acknowledges support from the NASA ROSES Cassini Data Analysis Program (NASA grant number G0500382) and the Planetary Data Archiving, Restoration, and Tools Program (NASA grant number G110546). The Cassini raw data sets are available on the NASA Planetary Data System (<https://science.nasa.gov/planetary-data-system>), and the processed wind and temperature fields of Saturn's atmosphere are available through Sayanagi et al., 2013 and Achterberg et al., 2014.

Appendix A. Thermodynamic parameters for Saturn

Saturn's gas constant, $R_{\text{gas}} = R^* / \bar{\mu}$, is calculated based on the universal gas constant, $R^* = 8.314463 \text{ J mol}^{-1} \text{ K}^{-1}$, and the mean molar mass, $\bar{\mu}$, of Saturn's upper troposphere. To calculate $\bar{\mu}$ we use up-to-date Cassini determinations of the concentrations of H_2 , He, and CH_4 , which together account for 99.9% of the dry atmospheric composition by volume. The mole fraction of CH_4 is taken to be 0.0047 (Fletcher et al., 2009). Based on a recent analysis by Achterberg and Flasar (2020), and their follow-up study (personal communication), the mole fractions of H_2 and He are taken to be 0.9302 and 0.0641, respectively. Combining these yields $\bar{\mu} = 2.2111 \text{ g mol}^{-1}$, such that $R_{\text{gas}} = 3760.12 \text{ J kg}^{-1} \text{ K}^{-1}$.

The potential temperature is defined as $\theta = T(p_s/p)^\kappa = T(p_s/p)^{R/c_p}$, where $\kappa = R_{\text{gas}}/c_p$, the specific heat capacity at constant pressure is c_p , and the reference pressure is $p_s = 1000 \text{ hPa}$. The heat capacities of He and CH_4 are taken to be 5192.87 and 2068.26 $\text{J kg}^{-1} \text{ K}^{-1}$, respectively. The heat capacity of H_2 , the dominant gas, is the net result of ortho and para molecular hydrogen, which act approximately like separate gases in Saturn's troposphere. We follow standard practice and assume “intermediate” hydrogen (Massie and Hunten, 1982), which is also known as “frozen equilibrium” hydrogen (Gierasch et al., 2004), using temperature-dependent profiles of the ratio of specific heat to gas constant provided by R. Achterberg (private

communication). From Fig. 2, the temperature at 400 hPa at latitude 40°N (i.e., the location of the 2010 storm) is 102.5 K, which corresponds to $(c_p/R_{\text{gas}})_{\text{H}_2} = 2.827$. The gas constant for H_2 is $4124.25 \text{ J kg}^{-1} \text{ K}^{-1}$, such that $c_p = 11659.25 \text{ J kg}^{-1} \text{ K}^{-1}$. The mass fractions are 0.8481, 0.1178, and 0.0341 for H_2 , He, and CH_4 , respectively. Combining the mass fractions and the heat capacities of these three gases, we calculate the net specific heat capacity in the vicinity of the 2010 storm to be $10545.01 \text{ J kg}^{-1} \text{ K}^{-1}$, such that $\kappa = 0.35658$.

References

- Achterberg, R.K., Flasar, F.M., 2020. Saturn's atmospheric helium abundance from Cassini composite infrared spectrometer data. *Planet. Sci. J.* 1, 30.
- Achterberg, R.K., et al., 2014. Changes to Saturn's zonal-mean tropospheric thermal structure after the 2010-2011 northern hemisphere storm. *Astrophys. J.* 786 <https://doi.org/10.1088/0004-637X/786/2/92>.
- Andrews, D.G., Holton, J.R., Leovy, C.B., 1987. *Middle Atmosphere Dynamics*. Academic, San Diego.
- Beron-Vera, F.J., Olascoaga, M.J., Brown, M.G., 2012. Zonal jets as meridional transport barriers in the subtropical and polar lower stratosphere. *J. Atmos. Sci.* 69, 753–767.
- Bevington, P.R., Robinson, D.K., 2003. *Data Reduction and Error Analysis for the Physical Sciences*, 3rd ed. McGraw-Hill Press, New York.
- Cao, H., Dougherty, M.K., Hunt, G.J., Provan, G., Cowley, S.W.H., Bunce, E.J., Kellock, S., Stevenson, D.J., 2019. The landscape of Saturn's internal magnetic field from the Cassini Grand Finale. *Icarus* 344, 113541.
- Dowling, T.E., 1995. Estimate of Jupiter's deep zonal-wind profile from Shoemaker-Levy 9 data and Arnold's second stability criterion. *Icarus* 117, 439–442.
- Dowling, T.E., 2019. Jets in planetary atmospheres. In: *Oxford Research Encyclopedia of Planetary Science*. <https://doi.org/10.1093/acrefore/9780190647926.013.116>.
- Dowling, T.E., 2020. Jupiter-style jet stability. *Planet. Sci. J.* 1, 6.
- Dritschel, D.G., McIntyre, M.E., 2008. Multiple jets as PV staircases: the Phillips effect and the resilience of eddy-transport barriers. *J. Atmos. Sci.* 65, 855–874.
- Fischer, G., et al., 2011. A giant thunderstorm on Saturn. *Nature* 475, 75–77.
- Flasar, F.M., et al., 2004. Exploring the Saturn system in the thermal infrared: the composite infrared spectrometer. *Space Sci. Rev.* 115, 169–297.
- Fletcher, L.N., Orton, G.S., Teanby, N.A., Irwin, P.G.J., Bjoraker, G.L., 2009. Methane and its isotopologues on Saturn from Cassini/CIRS observations. *Icarus* 199, 351–367.
- Fletcher, L.N., Achterberg, R.K., Greathouse, T.K., Orton, G.S., Conrath, B.J., Simon-Miller, A.A., Teanby, N., Guerlet, S., Irwin, P.G.J., Flasar, F.M., 2010. Seasonal change on Saturn from Cassini/CIRS observations, 2004-2009. *Icarus* 208, 337–352.
- Fletcher, L.N., et al., 2011. Thermal structure and dynamics of Saturn's northern springtime disturbance. *Science* 332, 1413–1417.
- García-Melendo, E., Pérez-Hoyos, S., Sánchez-Lavega, A., Hueso, R., 2011. Saturn's zonal wind profile in 2004–2009 from Cassini ISS images and its long-term variability. *Icarus* 215, 62–74.
- García-Melendo, E., et al., 2013. Atmospheric dynamics of Saturn's 2010 giant storm. *Nat. Geosci.* 23, 525–529. <https://doi.org/10.1038/NNGEO1860>.
- Gierasch, P.J., Conrath, B.J., Read, P.L., 2004. Nonconservation of Ertel potential vorticity in hydrogen atmospheres. *J. Atmos. Sci.* 61, 1953–1965.
- Holton, J.R., Hakim, G.J., 2013. *An Introduction to Dynamic Meteorology*, 5th ed. Academic, San Diego, California.
- Li, C., Ingersoll, A.P., 2015. Moist convection in hydrogen atmospheres and the frequency of Saturn's giant storms. *Nat. Geosci.* 5, 398.
- Massie, S.T., Hunten, D.M., 1982. Conversion of para and ortho hydrogen in the Jovian planets. *Icarus* 49, 213–226.
- McIntyre, M.E., 2014. Potential vorticity. In: North, G., Pyle, J., Zhang, F. (Eds.), *Encyclopedia of Atmospheric Science*, 2nd edition. Academic, San Diego.
- Pedlosky, J., 1987. *Geophysical Fluid Dynamics*. Springer-Verlag Press, New York.
- Polvani, L.M., Waugh, D.W., Plumb, R.A., 1995. On the subtropical edge of the stratospheric surf zone. *J. Atmos. Sci.* 52, 1288–1309.
- Porco, C.C., et al., 2004. Cassini imaging science: instrument characteristics and anticipated scientific investigations at Saturn. *Space Sci. Rev.* 115, 363–497.
- Read, P.L., et al., 2009a. Mapping potential vorticity dynamics on Saturn: zonal mean circulation from Cassini and Voyager data. *Planet. Space Sci.* 57, 1682–1698.
- Read, P.L., Dowling, T.E., Schubert, G., 2009b. Saturn's rotation period from its atmospheric planetary-wave configuration. *Nature* 460, 608–610.
- Salby, M.L., 1996. *Fundamentals of Atmospheric Physics*. Academic, San Diego.
- Sánchez-Lavega, A., Rojas, J.F., Sada, P.V., 2000. Saturn's zonal winds at cloud level. *Icarus* 147, 405–420.
- Sánchez-Lavega, A., et al., 2011. Deep winds beneath Saturn's upper clouds from a seasonal long-lived planetary-scale storm. *Nature* 475, 71–74.
- Sánchez-Lavega, A., et al., 2012. Ground-based observations of the long-term evolution and death of Saturn's Great White Spot. *Icarus* 220, 561–576.
- Sayanagi, K.M., et al., 2013. Dynamics of Saturn's great storm of 2010–2011 from Cassini ISS and RPWS. *Icarus* 223, 460–478.